Biophysical Journal
Article

Biophysical Society

Synaptophysin transmembrane domain III controls fusion pore dynamics in Ca^{2+}-triggered exocytosis

Yu-Tien Hsiao[1] and Meyer B. Jackson[1,*]
[1]Deptarment of Neuroscience, University of Wisconsin-Madison, Madison, Wisconsin

ABSTRACT Synaptophysin (syp) is a major protein of secretory vesicles with four transmembrane domains (TMDs) and a large cytoplasmic C-terminus. Syp has been shown to regulate exocytosis, vesicle cycling, and synaptic plasticity through its C-terminus. However, the roles of its TMDs remain unclear. The TMDs of soluble N-ethylmaleimide-sensitive factor attachment protein receptor (SNARE) proteins are thought to line initial fusion pores, and structural work together with sequence analysis suggest that TMD III of syp may play a similar role. To test this hypothesis, we performed tryptophan scanning experiments of TMD III in chromaffin cells and used amperometry to evaluate fusion pores. In contrast to SNARE TMDs, tryptophan substitutions in syp TMD III had no effect on the flux through initial fusion pores. However, a number of these mutants increased the fraction of kiss-and-run events and decreased the initial fusion pore lifetime. These results indicate that TMD III stabilizes the initial fusion pore and controls the initial choice between kiss and run and full fusion. Late-stage fusion pores were not impacted by TMD III mutations. These results indicate that syp TMD III does not line the initial fusion pore. However, its impact on pore dynamics suggests that it interacts with a SNARE protein implicated as a part of the fusion pore that forms at the onset of exocytosis.

SIGNIFICANCE The integral membrane protein synaptophysin is highly abundant on synaptic and dense-core vesicles. The third of synaptophysin's four transmembrane domains has been hypothesized on the basis of sequence homology and structural analysis to form a channel. Amperometry measurements of fusion pore flux from dense-core vesicles in endocrine cells were conducted with tryptophan mutations in the implicated transmembrane domain. These results negated the hypothesis that this domain lines the fusion pore but revealed a strong control over the stability of the initial fusion pore and the choice of release mode. Thus, while the third transmembrane domain does not line the initial fusion pore, its influence on pore dynamics suggests that it interacts with other proteins that do.

INTRODUCTION

Calcium-triggered exocytosis underlies the release of chemical signals throughout the nervous and endocrine systems. The coordinated activity of a key set of proteins drives the fusion of the vesicle and plasma membranes under tight temporal control. This process begins with the opening of a fusion pore that allows a low flux of vesicle content (1,2). Based on the sensitivity of fusion pore flux to transmembrane domain (TMD) mutations, it has been proposed that this initial pore is formed by the TMDs of two soluble N-ethylmaleimide-sensitive factor attachment protein receptors (SNAREs), syntaxin and synaptobrevin (syb) (3–7). SNARE proteins also control the dynamics of initial fusion pores (8–12), as do SNARE-interacting proteins, such as synaptotagmins (13–16) and cysteine-string protein (17). Synaptophysin (syp), a tetraspanner protein (18) that is abundant on synaptic vesicles (19,20) and dense-core vesicles (DCVs) (21,22), has been shown to control fusion pore dynamics (23), but many of its roles in exocytosis are unclear. Synapse morphology and synaptic transmission appear normal in the absence of syp, and the levels of other exocytosis proteins are unaltered (24–26), but double knockouts (DKOs) lacking both syp and another tetraspanner, synaptogyrin (syg), display impaired synaptic plasticity (26). Syp KO chromaffin cells show very little reduction in DCV release, but secretion is reduced twofold in DKO cells (23).

Tetraspanners such as syp and syg harbor four TMDs and a large cytoplasmic C-terminus. The C-terminus influences the time course of catecholamine efflux during DCV exocytosis (21), controls late-stage fusion pores (23), and regulates the kinetics of synaptic vesicle endocytosis (27). However, the functions for the TMDs of syp have not been established. Purified syp forms hexameric channel-like

Submitted June 16, 2022, and accepted for publication September 23, 2022.
*Correspondence: meyer.jackson@wisc.edu
Editor: Ben O'Shaughnessy.
https://doi.org/10.1016/j.bpj.2022.09.029

structures (28) and may produce channels in lipid membranes (29). Syp has a similar overall TMD topology to connexins, which form gap-junction channels (30–32). TMD III of connexin lines gap junction pores and has alternating hydrophobic residues. TMD III of syp displays a similar pattern (30) and has a weak sequence homology with connexin TMD III (28,31). In a complex containing six copies of syp and 12 copies of syb, TMDs III and IV of syp partner with the TMD of syb to line a central aqueous cavity (32). In this complex, the residues of syb that face inward include those that alter catecholamine flux through endocrine fusion pores (5,33) and glutamate flux through synaptic fusion pores (3). These studies raise important questions about the role of tetraspanner proteins in fusion pores. If a cavity like that seen in the syb-syp structure of Adams et al. (32) forms at the onset of fusion, then syp TMD III would be a pore liner and influence pore flux in a manner similar to that seen with the SNARE TMDs.

To address these questions, we tested syp TMD III tryptophan mutants in chromaffin cells and used amperometry to assess their impact on fusion pores during calcium-triggered DCV exocytosis. DKO cells provide an advantageous background for these studies because they lack two major endogenous tetraspanners that could obscure the effects of exogenous mutants. We found that TMD III mutants support exocytosis in DKO chromaffin cells but alter initial fusion pore dynamics and mode of release. Tryptophan substitutions throughout TMD III failed to alter catecholamine flux through the initial fusion pore, indicating that this domain is not a pore liner. Thus, the pore-like syp-syb complex (32) does not represent the initial fusion pore of Ca^{2+}-triggered exocytosis, but interactions between these two proteins stabilize fusion pores and determine how they evolve as exocytosis progresses.

MATERIALS AND METHODS

Animals

Breeding homozygous syp KO/heterozygous syg KO mice generated litters with ~25% DKO (25,26). DKO offspring were identified by genotyping. All mice were housed and handled in accordance with the guidelines of the National Institutes of Health and approved by the Animal Care and Use Committee of the University of Wisconsin-Madison.

Chromaffin cell culture

Chromaffin cells were prepared as described previously (23). Mouse adrenal glands were collected in ice cold Hanks' balanced salt solution with penicillin/streptomycin, cut into small pieces, and dissociated in DMEM with 20 U papain, 10 mg L-cysteine, 0.02 M $CaCl_2$, and 0.02 M EDTA at 37°C for 25 to 30 min. After replacing the papain solution with enriched medium (DMEM with insulin-transferrin-selenium-X and penicillin/streptomycin), the tissue was triturated and plated on glass coverslips coated with poly-D-lysine for 1 h. One mL enriched medium was added, and cells were maintained in an incubator at 37°C ventilated with a humidified air-5% CO_2 atmosphere.

Molecular biology

Point mutations with tryptophan in TMD III were generated by modified sequential PCR (34) with rat wild-type syp (pLox-CMV-syp-IRES2-EGFP) as the template. Primers were designed with the QuickChange Primer Design Program (Agilent Technologies, Santa Clara, CA, USA). Constructs were confirmed by DNA sequencing, subcloned into a bicistronic lentiviral vector, pLox-CMV-IRES-EGFP, and purified. Lentivirus particles were generated in HEK 293T cells as described previously (23). DKO chromaffin cells were infected with virus particles on the day of dissection. Amperometry recordings were conducted 48–72 h after viral infection.

Amperometry

Chromaffin cells were recorded in bathing solution with 150 mM NaCl, 4.2 mM KCl, 1 mM NaH_2PO_4, 0.7 mM $MgCl_2$, 2 mM $CaCl_2$, and 10 mM HEPES (pH 7.4) at room temperature (22°C). Secretion was induced by pressure ejection of a depolarizing solution consisting of 105 mM KCl and 2 mM NaCl from a 2-μm tipped micropipette positioned 15–20 μm away from the cell under study. Catecholamine-oxidization currents were recorded with a 5-μm diameter-tipped carbon fiber electrode (CFE-2, ALA Scientific Instruments, Farmingdale, NY, USA) polarized at 650 mV with a VA-10× amplifier (ALA Scientific Instruments). The carbon fiber electrode tip was cut to expose fresh surface between recordings from different cells. Signals were low-pass filtered at 1 kHz and read into a computer at a digitization rate of 4 kHz with pClamp10 (Axon Instruments, Molecular Devices, Silicon Valley, CA, USA). Depolarizing solution was applied 3 s after the start of acquisition for 6 s, and recording continued for another 14 s (total time: 23 s). Each cell was stimulated six times. Data analysis was conducted with an in-house computer program. Events with peak amplitude $\geq$2 pA were located and analyzed. Events 2–4 pA were taken as kiss and run, while events $\geq$4 pA were taken as full fusion. Spike frequency was calculated for events $\geq$4 pA from the first secretion episode of each cell. Rising slopes were obtained by linear regression of the 10%–70% rising phase of cumulative spike-count plots. Prespike feet (PSFs) were analyzed from spikes $\geq$20 pA. PSF lifetime was determined using the criteria of Chow and von Rüden (35), and amplitude was determined by dividing area by lifetime (5). Mean PSF duration was determined by fitting lifetime distributions with a single exponential decay. Spike characteristics and late-stage permeability were analyzed from spikes with peak amplitudes $\geq$20 pA using methods described previously (36).

Immunocytochemistry and confocal imaging

DKO chromaffin cells were cotransfected with wild-type (WT) or mutant syp together with neuropeptide Y-DsRed (NPY-DsRed). Cells were fixed 72 h after transfection with 4% paraformaldehyde for 30 min, permeabilized with 0.1% Triton X-100, and blocked in 10% goat serum for 1 h, all at room temperature (RT). Cells were then incubated at 4°C overnight with rabbit anti-syp antibody (Synaptic Systems, Göttingen, Germany, #101002) and mouse anti-syb antibody (Synaptic Systems #104211) or mouse anti-RFP antibody (Thermo Fisher Scientific, Waltham, MA, USA, #MA5-15257) at a dilution of 1:280. After washing three times with phosphate-buffered saline for 10 min, cells were incubated with AF568-goat anti-mouse (Abcam, Waltham, MA, USA, #ab175473) and AF647-goat anti-rabbit (Sigma-Aldrich, Burlington, MA, USA, #SAB4 600185) antibodies or AF647-goat anti-mouse (Sigma #SAB4600392) and AF546-goat anti-rabbit (Invitrogen #A11010) antibodies at 1:1,000 dilution at RT for 1 h. Cells were then washed three times with phosphate-buffered saline for 10 min and incubated with DAPI at RT for 10 min. The coverslips were sealed onto slides with Fluoromount G (Electron Microscopy Sciences, Hatfield, PA, USA). Cells were imaged with a Leica TCS SP8 laser-scanning confocal microscope equipped with a 63× oil immersion lens. The laser intensity was set to 12% for 561 and

633 nm and 5% for 405 nm. Pearson's correlation coefficient was determined by Leica application suite X colocalization software.

Statistics

All data were presented as mean ± SE. Means of spike frequency, spike characteristics, PSF amplitude, fraction of kiss-and-run events, kiss-and-run duration, and permeability of fusion pores were reported as the cell means, with averages first taken over each cell and then averaging these means; cell number was used to calculate error (37). One-way ANOVA followed by post hoc Student-Newman-Keuls test or the Kruskal-Wallis method followed by post-hoc Dunn test was used to evaluate statistical significance among different test groups. The significance was represented with asterisks with the following notation: *$p < 0.05$; **$p < 0.01$; ***$p < 0.001$. All data and statistical analyses were performed with the computer programs Origin and GraphPad.

RESULTS

Syp TMD III mutants support secretion

To investigate the role of syp TMD III, we expressed syp mutants in DKO cells lacking syp and its homolog syg. The ablation of these proteins does not lead to changes in the expression levels of other major exocytosis proteins (26), and their absence permits exogenous mutants to have an impact. We replaced 12 different residues of syp TMD III with tryptophan (Fig. 1 *A*, *open boxes*) and expressed each of these mutants in DKO chromaffin cells. Most of these residues appear to face into the lumen of the pore in the syb-syp structure (32). Fig. 1 *A* shows that our mutations extended over the length of TMD III. The syb TMD residues that influence pore flux are concentrated toward the N-terminus near the cytoplasm (5), and we anticipated that the syp TMD III could fill in the gap toward the vesicle lumen. Therefore, our syp TMD III mutations covered this region more thoroughly.

To confirm that exogenous WT syp and tryptophan mutants target DCVs, we coexpressed NPY-DsRed to mark DCVs in DKO cells and evaluated colocalization with syp by immunocytochemistry. Fig. 1 *B* showed that WT syp and selected mutants (green) colocalized with NPY-DsRed (red), and the Pearson's coefficient was not significantly different between syp and mutants (Fig. 1 *C*). This confirms the presence of syp on DCVs (21–23) and suggests that our syp mutants target DCVs as effectively as WT. Since syp associates with syb and syb targets to DCVs (5), we also checked the colocalization of syp and syb. As expected, WT and mutant syp (red) colocalized with syb (green) (Fig. 1 *D*), and the Pearson's coefficients were indistinguishable between WT syp and mutants (Fig. 1 *E*). Note that the Pearson's coefficient with syb in Fig. 1 *A* was higher than that with NPY in Fig. 1 *C*, suggesting that syp targets some structures that are not DCVs, such as small clear vesicles. These results suggest that exogenous WT and mutant syp efficiently target DCVs.

We then used amperometry to test the impact of these mutants on exocytosis. Fig. 2 *A* presents amperometry recordings from control DKO cells and DKO cells expressing WT syp, syg, and three mutants. Upon depolarization, untransfected DKO cells and DKO cells expressing WT syp or syg secrete, as indicated by the amperometric spikes evident in each trace. Thus, although DKO cells lack the two major tetraspanners, they do not provide a secretion-free background, possibly due to redundancy of function with other tetraspanners or to tetraspanner-independent secretion. Secretion varies from cell to cell, so the frequency was averaged over cells (Fig. 2 *B*). The mean spike frequency did not have a statistically significant dependence on syp form (by ANOVA), and frequencies were generally roughly half that seen in WT chromaffin cells (23). Tryptophan substitution in the N-terminal part of TMD III tended to increase frequency, while substitutions that reduced frequency were only found in the C-terminus (Fig. 2 *B*). Cumulative plots of spike number versus time provide another view of spike frequency by focusing on the 10%–70% rising slope (Fig. 2 *C*). This analysis indicated some variation depending on the position of the tryptophan substitution: most mutants toward the N-terminus produced a higher rising slope, while three mutants toward the C-terminus (L149, V150, and S151) reduced the rising slope (Fig. 2 *D*). One mutant near the C-terminus (S152) produced a small increase in rising slope. Note that spike frequency (Fig. 2 *B*) provides a more conservative analysis based on cell mean, whereas rising slope (Fig. 2 *D*) combines the total number of spikes without taking a cell mean. Thus, the error of rising slope is smaller because it ultimately depends on the much larger event number. The appropriateness of event-based and cell-based statistical analysis of amperometry data depends on the contribution of variation between cells to the total variance (23,37). With this qualification, the results indicate that these tryptophan mutants exert neither a large dominant-negative action nor a rescue action. However, the parallel trends in spike frequency and rising slope, and the clustering of similar actions, suggest that tryptophan substitutions toward the N-terminus can enhance secretion, while substitutions toward the C-terminus can inhibit secretion.

Changes in kiss-and-run fraction and duration

Exocytosis begins with the opening of a fusion pore. Upon opening, a fusion pore can either dilate or close. Following dilating, the fusion pore can then shrink and close (38,39) or possibly expand further with full fusion and merger of the vesicle and plasma membranes. Dilation leads to secretion of a larger fraction of vesicle content, while closure prior to dilation limits loss to a smaller fraction of content in a distinct form of early kiss and run. In amperometry recordings, dilation of the initial fusion pore results in spikes, while closure of the initial fusion pore results in stand-alone feet, which are early kiss-and-run events similar in amplitudes to PSFs (40,41).

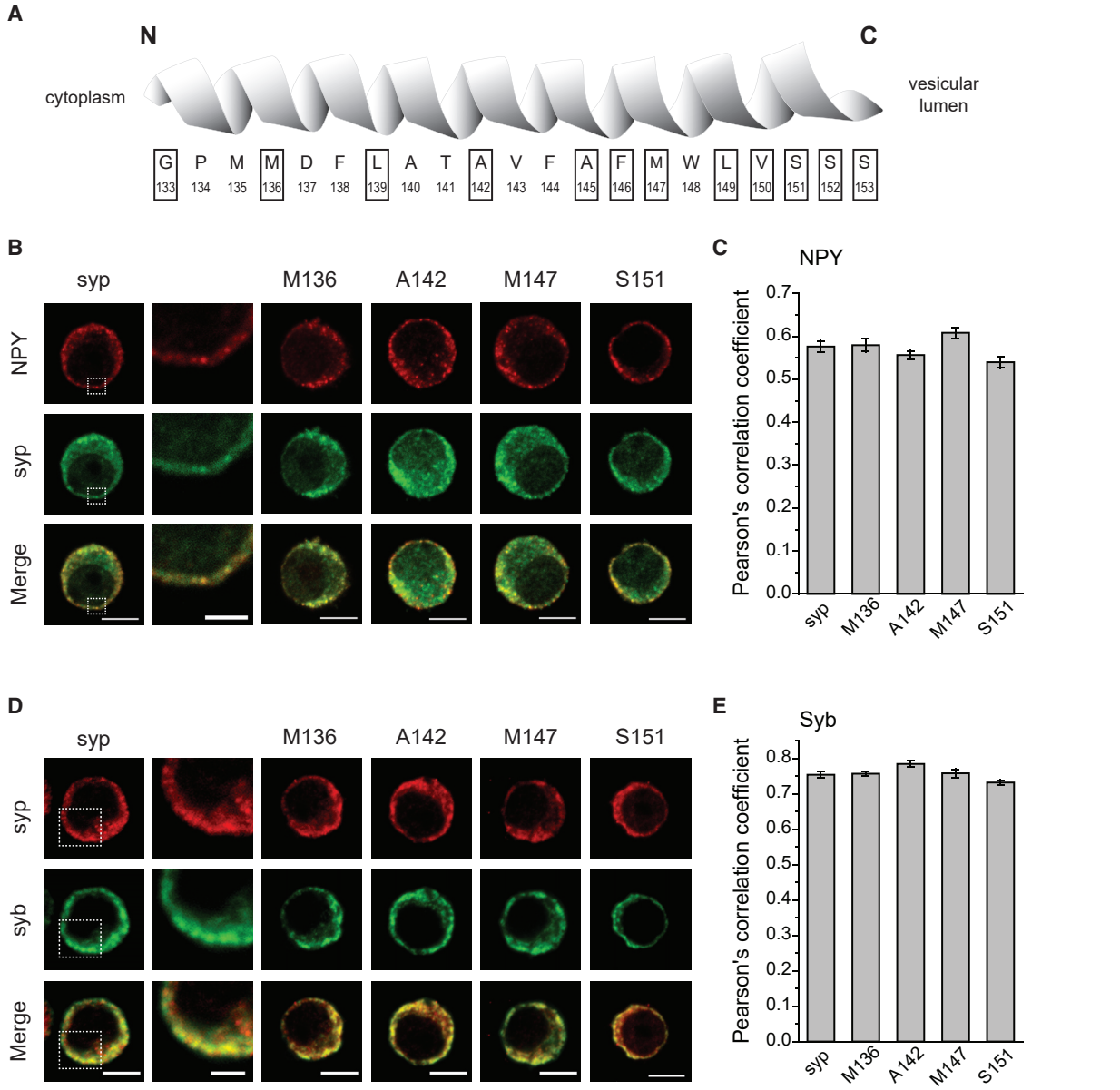

FIGURE 1 Vesicle targeting by wild-type and mutant syp. (*A*) Residues of syp TMD III. The residues replaced with tryptophan are indicated by open boxes. (*B*) Immunostaining images of NPY-DsRed (*red*) and syp (*green*) in DKO chromaffin cells cotransfected with NPY-DsRed and wild-type syp or with the indicated syp tryptophan mutants. The images to the right of the syp column are expanded views of the region in the white rectangle. (*C*) Pearson's correlation coefficient for colocalization of syp and NPY. (*D*) Immunostaining of syp (*red*) and syb (*green*) in DKO chromaffin cells transfected with wild-type syp or tryptophan mutants. As in (*B*), the images to the right of the syp column are expanded views of the region in the white rectangle. (*E*) Pearson's correlation coefficient for colocalization of syp and syb. $N = 18–28$ cells. Error bars represent standard error of the mean. Scale bars: 5 μm in all panels except in the magnified regions to the right of the syp column, where the scale bars are 2 μm.

Fig. 3 *A* displays examples of kiss-and-run events from control DKO chromaffin cells and DKO chromaffin cells expressing two mutants. The sorting of events into two populations corresponding to full fusion and early kiss-and-run has been validated using an objective cutoff based on spike shape (42). Classifying events by either cutoffs of 4 or 6 pA, or by spike shape, generally preserves differences between cells expressing different proteins (23,42). Here, we used the 4 pA cutoff, calculated the fractions of kiss-and-run versus full-fusion events for each cell, and averaged this fraction to obtain the cell mean. Syp KO cells and DKO cells displayed higher fractions of kiss-and-run events, suggesting that syp can influence the choice between kiss-and-run and full fusion (23). DKO cells expressing syg showed a comparable fraction to control DKO cells (Fig. 3 *B*), suggesting that syg has little, if any, influence on release mode. Tryptophan replacement of M136, L139, and A142 significantly increased this fraction (Fig. 3 *B*). Furthermore,

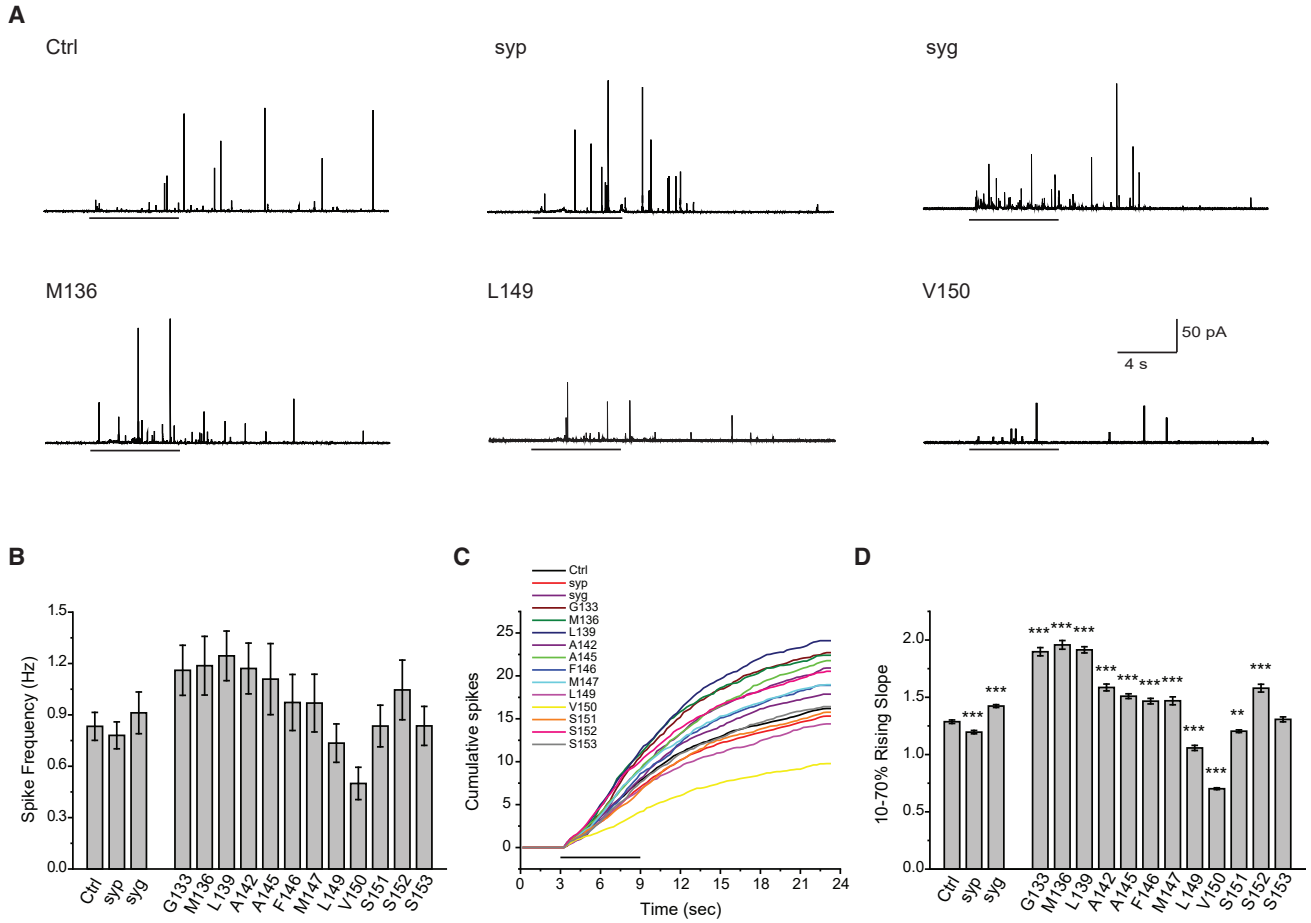

FIGURE 2 Spike frequency. (*A*) Traces of amperometry recordings from DKO cells expressing empty vector (Ctrl), wild-type syp, syg, and tryptophan mutants. Black horizontal lines below indicate application of depolarizing high KCl solution. (*B*) Mean spike frequency averaged over cells. There were no significant differences between these groups. Error bars represent standard error of the mean. (*C*) Cumulative spike counts were plotted versus time, with the black line below indicating high KCl application (as in *A*). (*D*) 10%–70% rising slopes of cumulative plots determined from linear fits. Data were 1,685 spikes from 103 cells for Ctrl; 1,164 spikes from 76 cells for wild-type syp; 804 spikes from 45 cells for syg; 314–784 spikes from 20–41 cells for mutants. Error bars represent errors of the slope from the linear fit. **p $<$ 0.01; ***p $<$ 0.001, Kruskal-Wallis method followed by post-hoc Dunn test.

these same three mutants increased the duration of kiss-and-run events compared with other mutants, control DKO cells, and WT syp and syg (Fig. 3 *C*). This suggests that this part of syp TMD III plays a role in stabilizing the fusion pore responsible for early kiss and run.

Initial fusion pore stability

When the opening of a fusion pore leads to a spike, the initial small current is referred to as a PSF (Fig. 4 *A*, *gray area*) (1,2). To determine the role of TMD III in the stability of these initial fusion pores, we examined PSFs in DKO cells expressing tryptophan mutants. The mean PSF duration was determined by fitting a single exponential to the PSF lifetime distribution (Fig. 4 *B*). These values were similar in control and WT syp-expressing DKO cells but were shorter in syg-expressing DKO cells (Fig. 4 *C*), suggesting that syg destabilizes the initial fusion pore. Four tryptophan mutants, M136, F146, L149, and S153, produced large changes in mean PSF duration, and in each case, the duration was reduced (Fig. 4 *C*). This suggests that these four residues engage in interactions that stabilize the initial fusion pore and that tryptophan replacement disrupts these interactions.

Initial fusion pores flux

The findings that syp and syb form a complex (43) with a hexameric pore-like structure (32) and that syp TMD III has a transmembrane topology similar to connexin TMD III (30,31) raise the possibility that TMD III serves as a structural component of a fusion pore. Catecholamine flux can be used to probe the size of a pore, and tryptophan TMD mutations in SNAREs have been shown to reduce PSF amplitudes (5,7). We therefore examined the PSF amplitudes in DKO cells expressing syp TMD III mutations.

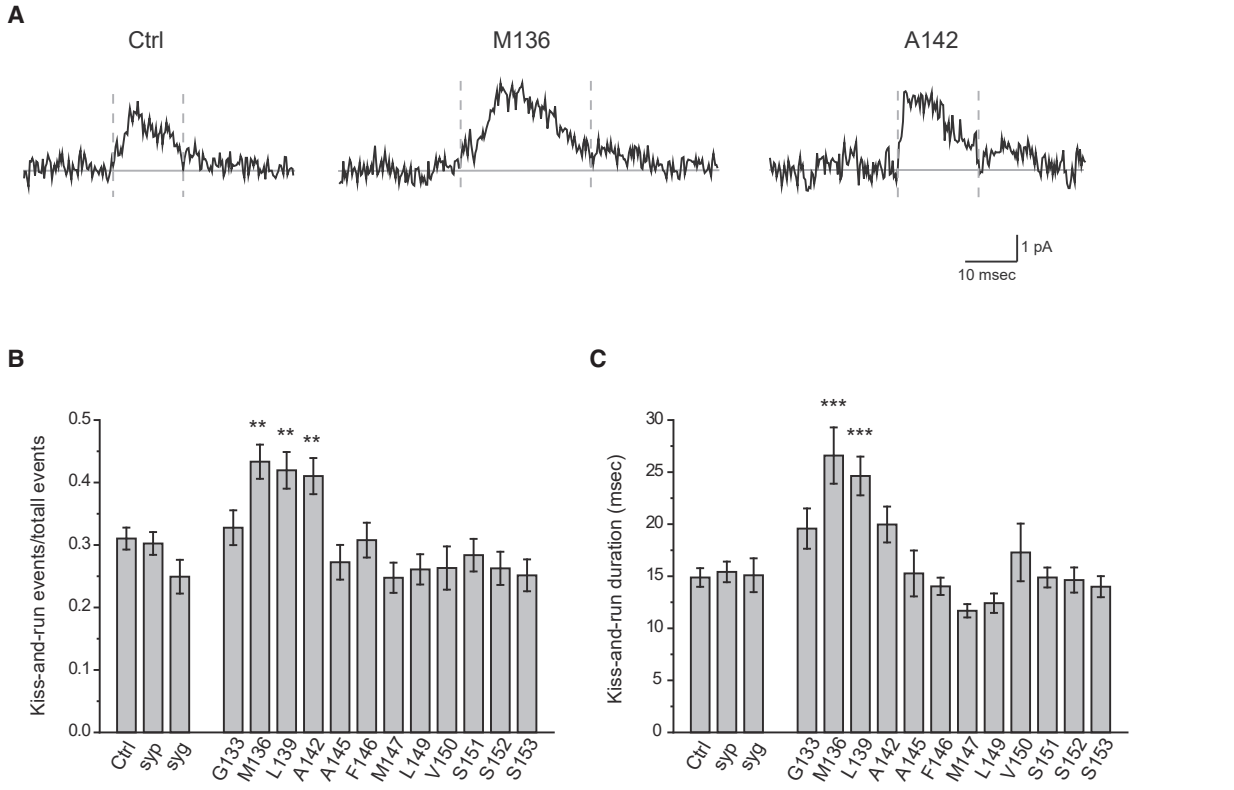

FIGURE 3 Kiss and run events. (*A*) Amperometric recordings from Ctrl DKO cells and DKO cells expressing two different tryptophan mutants. (*B*) Fraction of kiss-and-run events was calculated from events with peak amplitudes of 2–4 pA relative to the total events with peak amplitude $\geq$2 pA. C. Kiss-and-run duration in all test groups. 2288 events from 103 cells for Ctrl; 1476 events from 76 cells for wild type syp; 832 events from 45 cells for syg; 302–1263 events from 20 to 41 cells for mutants. Error bars represent standard error of the mean. **p $<$ 0.01; ***p $<$ 0.001, One-way ANOVA followed by post hoc Student-Newman-Keuls test.

None of the mutants produced statistically significant changes in PSF amplitude (Fig. 4 *D*). By contrast, three TMD mutations in syntaxin (7) and four TMD mutations in syb (5) produced statistically significant reductions in PSF amplitude. The finding that tryptophan substitutions in TMD III of syp do not influence catecholamine flux through the initial fusion pore indicates that this domain does not reside near the aqueous exit pathway taken by catecholamine during its release.

Spike shape and fusion pore expansion

The dilation of the initial fusion pore produces the amperometric spike, the shape of which depends on the properties of the late-stage pore formed by expansion of the initial fusion pore. The C-terminus of syp has been shown to influence spike shape by changing the late-stage pore (23). We evaluated various indices of spike shape illustrated in Fig. 5 *A*. None of the TMD III mutants had a significant impact on spike amplitude (Fig. 5 *B*), 35%–90% rising time (Fig. 5 *C*), half-width (Fig. 5 *D*), decay time (Fig. 5 *E*), or whole area (Fig. 5 *F*). To relate spike shape to late-stage fusion pores, we calculated permeability as the ratio of amperometric current to remaining vesicle catecholamine content (36). As shown previously, fusion pore permeability rises suddenly at the start of dilation and, after reaching a peak, decays to a plateau (Fig. 6 *A*). The peak and plateau fusion pore permeabilities were statistically indistinguishable for the various proteins and mutants examined here (Fig. 6 *B* and *C*). These results show that TMD III does not regulate late-stage fusion pores. Thus, the influence of syp on spike shape and late-stage fusion pores (23) is more likely to reflect an action of the C-terminus in determining whether late-state pores expand or close.

DISCUSSION

Roles for tetraspanners in membrane fusion during exocytosis have proven difficult to identify. Overexpressing syp or syg in PC12 cells downregulates human growth hormone release (44). Depleting neuronal syp and syg increased synaptic vesicle release at the calyx of Held synapse (45). In *Drosophila*, eliminating syg reduced spontaneous synaptic release (46), but *C. elegans* tetraspanner-null mutants displayed normal miniature postsynaptic currents (47). Redundant actions of different isoforms make it difficult to evaluate the results of KO experiments, and species differences add to the challenge of determining general functions. We recently

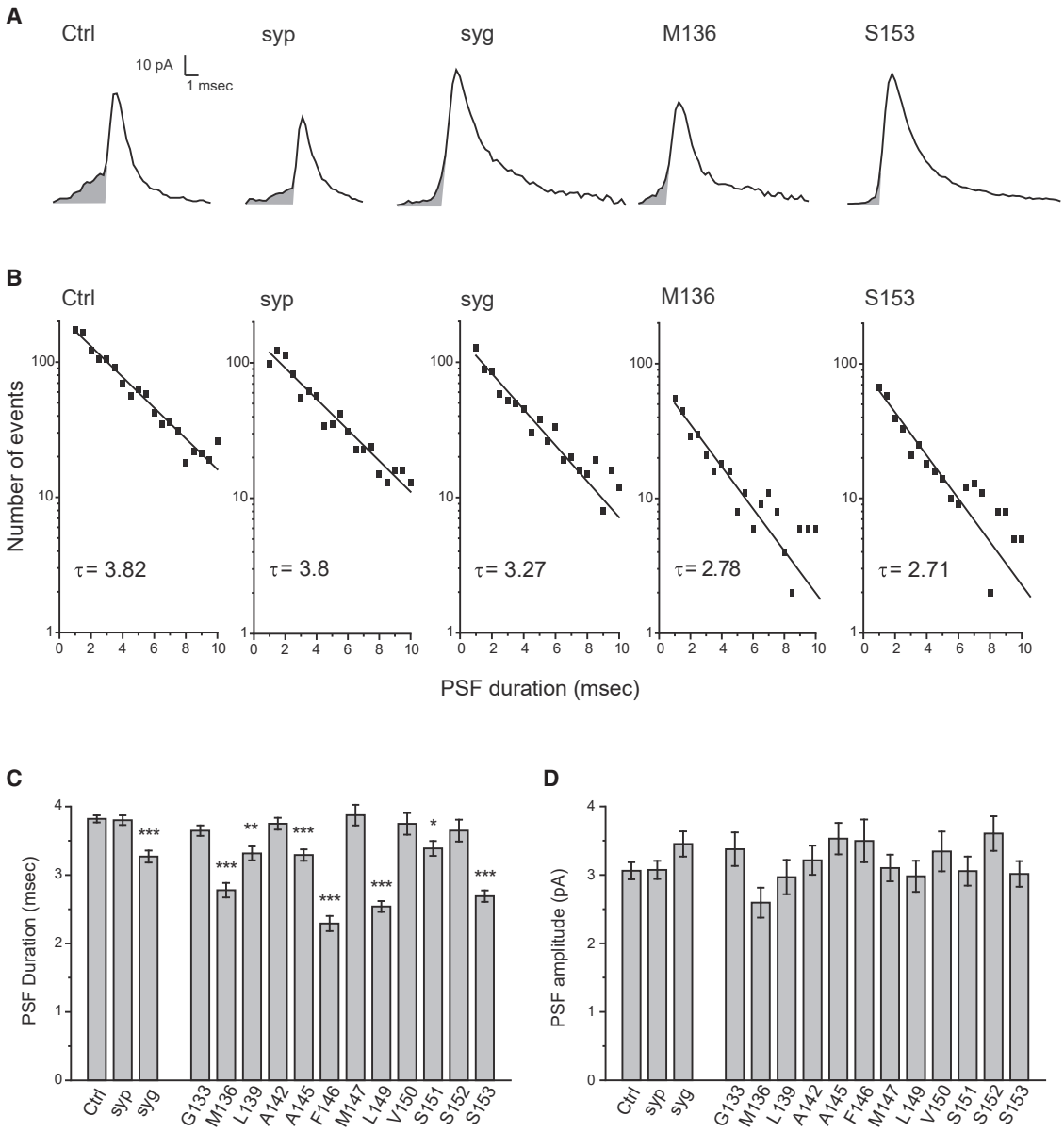

FIGURE 4 Prespike feet. (*A*) Amperometric spikes from Ctrl, syp, syg, and two tryptophan mutants, M136 and S153. PSFs are indicated as gray shaded regions. (*B*) Lifetime distribution of PSF was fitted with a single exponential decay function to yield τ, the mean PSF duration. (*C*) Mean of PSF duration from the fits as in (*B*). Error bars represent errors determined from exponential fits. (*D*) Cell mean of PSF amplitude (1,500 events from 103 cells for Ctrl; 1,031 events from 76 cells for syp; 871 events from 45 cells for syg; 249–700 events from 20–41 cells for mutants). Error bars represent the standard error of the mean. *$p < 0.01$; **$p < 0.01$; ***$p < 0.001$, one-way ANOVA followed by post hoc Student-Newman-Keuls test.

found that syp protein level and secretion were not well correlated (23). Here, we showed that heterologous syp and syg do not enhance secretion above that seen in DKO cells (Fig. 2). Experiments with a syp deletion mutant had suggested different functions for the C-terminus and TMDs (23), prompting us to investigate the TMDs in more detail. We focused on TMD III, a domain with a potential role as a fusion pore component. Tryptophan substitutions in TMD III did not alter flux through initial or late-stage fusion pores. Mutations at specific locations did, however, influence the stability of initial fusion pores and the mode of exocytosis. Thus, although it does not line the fusion pore, TMD III controls functionally important fusion pore transitions in early stages of calcium-triggered exocytosis in endocrine cells. Syp is also highly abundant on synaptic vesicles (19,20), where an impact on initial fusion pores could play a role in the dynamics of synaptic release.

Syp TMD III and initial fusion pore composition

Our experiments tested the hypothesis that TMD III of syp lines the initial fusion pore. Syp interacts with syb to form

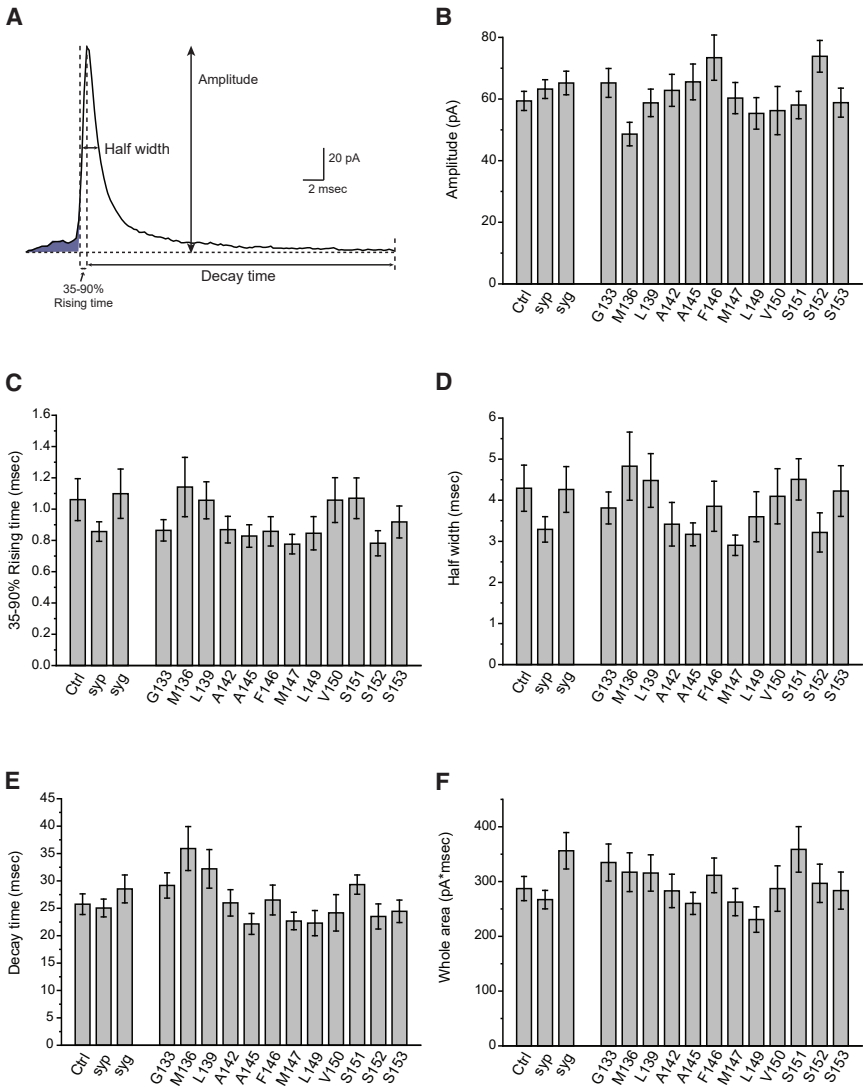

FIGURE 5 Spike characteristics. (*A*) An amperometry spike with PSFs shaded and key parameters illustrated. (*B–F*) Cell means of peak spike amplitude (*B*), 35%–90% rise time (*C*), half-width (*D*), decay time (*E*), and total area (*F*). Values were cell means calculated from spikes with peak amplitude $\geq$20 pA. Error bars represent standard error of the mean. Spike and cell numbers as in Fig. 4.

a stoichiometric complex with a channel-like structure (32). If this complex represents an initial fusion pore, tryptophan mutants in TMD III that face into the pore lumen would be expected to reduce the amplitude of the PSF (Fig. 4 *D*). The failure of these mutations to alter initial fusion pore flux suggests that these residues do not interact with permeating catecholamine. This indicates that despite the homologies with connexin (30,31), it is unlikely that TMD III lines the initial fusion pore. The syp-syb complex characterized by Adams et al. (32) is therefore unlikely to represent the initial fusion pore, but other functions remain a possibility.

Syp TMD III and fusion pore dynamics

Although not a pore liner, TMD III does nevertheless influence initial fusion pores. TMD III mutations altered the stability of the initial fusion pore (Fig. 4 *B*), as well as fusion pores associated with early kiss-and-run (Fig. 3 *B* and *C*). A direct interaction of TMD III with components of the initial fusion pore within the membrane is the most parsimonious interpretation of these results. However, TMD III mutations could alter syp binding to syb to influence its availability or trafficking (48). An interaction between TMD III and the C-terminal cytoplasmic domain of syp cannot be ruled out, and a change in the conformation of this domain could alter its association with dynamin (21). However, syp C-terminus deletion does not alter PSF lifetime (23), so it is unlikely that the actions of TMD III mutations on PSF reported here depend on the C-terminus. The effects reported here are specific to initial fusion pores, as spike shape and late-stage fusion pore permeability were not affected (Figs. 5 and 6). Thus, TMD III has little, if any, impact on the closure of fusion pores after they have dilated (38,39). Changes in the proportion and lifetime of early kiss-and-run events indicate an additional role in the choice of release mode made by the initial fusion pore (Fig. 3). It is notable that mutations that destabilize initial fusion pores also stabilize kiss-and-run events. This can be

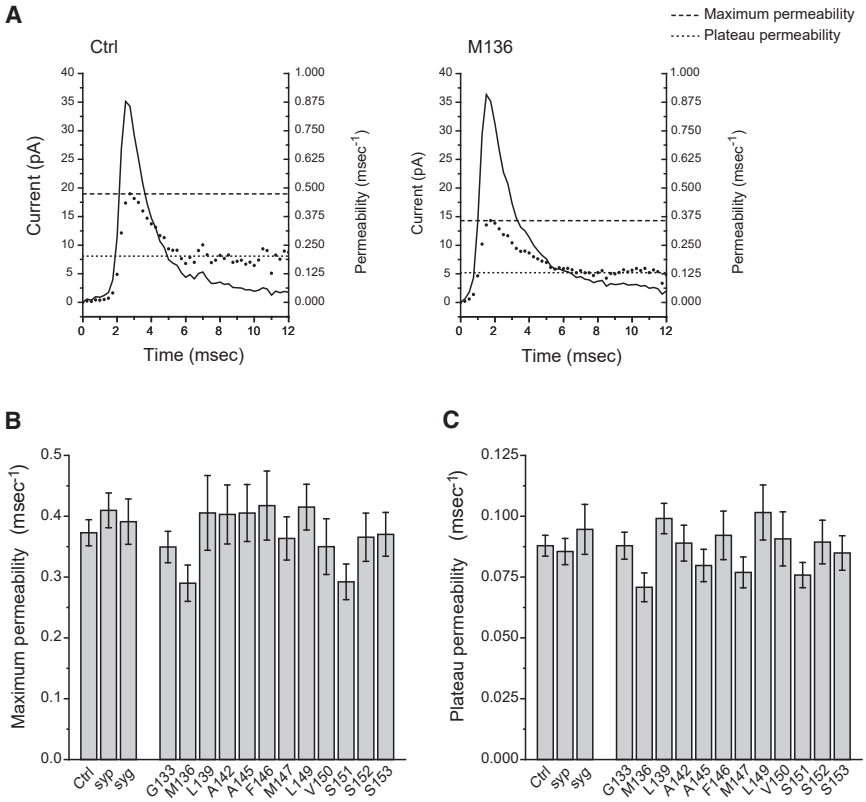

FIGURE 6 Late-stage fusion pores. (*A*) Permeability (*dotted trace*) was calculated by using amperometric currents (*solid trace*) as described previously (36). Peak permeability and plateau permeability are indicated with dashed and dotted lines, respectively. (*B*) Average peak permeability. (*C*) Average plateau permeability. Values are cell means, with spike and cell numbers as in Figure 4 and error bars representing standard error of the mean.

seen by comparing the impact of residues M136 and L139 on the PSF lifetime (Fig. 4 *C*) and kiss-and-run event lifetime (Fig 3 *B*). The briefer PSFs reflect an acceleration of the transition to a second fusion pore state formed by an irreversible transition of the initial fusion pore (42). These mutations destabilize the first state and stabilize the second state, suggesting that TMD III is arranged differently in these two fusion pore states. In contrast to residues M136 and L139, four other residues extending toward the vesicle lumen destabilize PSFs without altering kiss-and-run events, and these residues had the largest effects. This suggests that this part of syp TMD III has interactions that selectively stabilize initial fusion pores of PSFs but do not stabilize the fusion pore after bifurcation to the downstream state that cannot dilate (42).

Interestingly, the three residues implicated in the control of release mode are located close to the cytosolic face of the vesicle membrane. Tryptophan substitutions within the syb TMD perturb the surrounding lipid bilayer and alter membrane curvature (49). Tryptophan substitutions in syp TMD III could similarly impact the stability of a lipidic fusion pore and thus influence dilating transitions from an initial proteinaceous fusion pore. This may also be relevant to the trend evident in the spike frequency data (Fig. 2), where mutations toward the cytoplasm were observed to increase spiking, while residues toward the lumen were observed to reduce spiking. A previous study indicated that the syp C-terminus influences the initial choice between full-fusion and kiss-and-run (23). The present results suggest that both TMD III and the C-terminus of syp impact this choice. By contrast, the stability of the initial fusion pore depends primarily on TMD III. It is not a pore liner itself but may interact with pore-lining domains of other proteins.

TMD interactions between syp and syb

The most likely interacting partner for syp in the vesicle membrane is syb, as these two molecules have a well-documented interaction (32,43,50,51). To explore the possible relevance of syp-syb interactions to our present results on syp, we revisited prior results with syb (5). Helical wheels (Fig. 7 *A*1) illustrate that residues of syb that influence PSF lifetime are distributed through most of its TMD; likewise, the seven residues of syp TMD III that influence PSF lifetime are also distributed. By contrast, residues that influence early kiss-and-run event lifetime tend to be situated on one broad helical face (Fig. 7 *A*2).

To explore interactions between these TMDs in greater detail, we examined structural data and models. In the electron microscopy structure that motivated the present study (32), five of the seven residues of syp with an effect on PSF lifetime (L139, A145, F146, L149, and S153) face away from the syb TMD and toward the syp TMD IV (included in Fig. 7 *B*1) or toward syp TMD I (data not shown). Two residues of TMD III with an effect on PSF lifetime, M136 and S151, are close to syb in this model. Because the electron

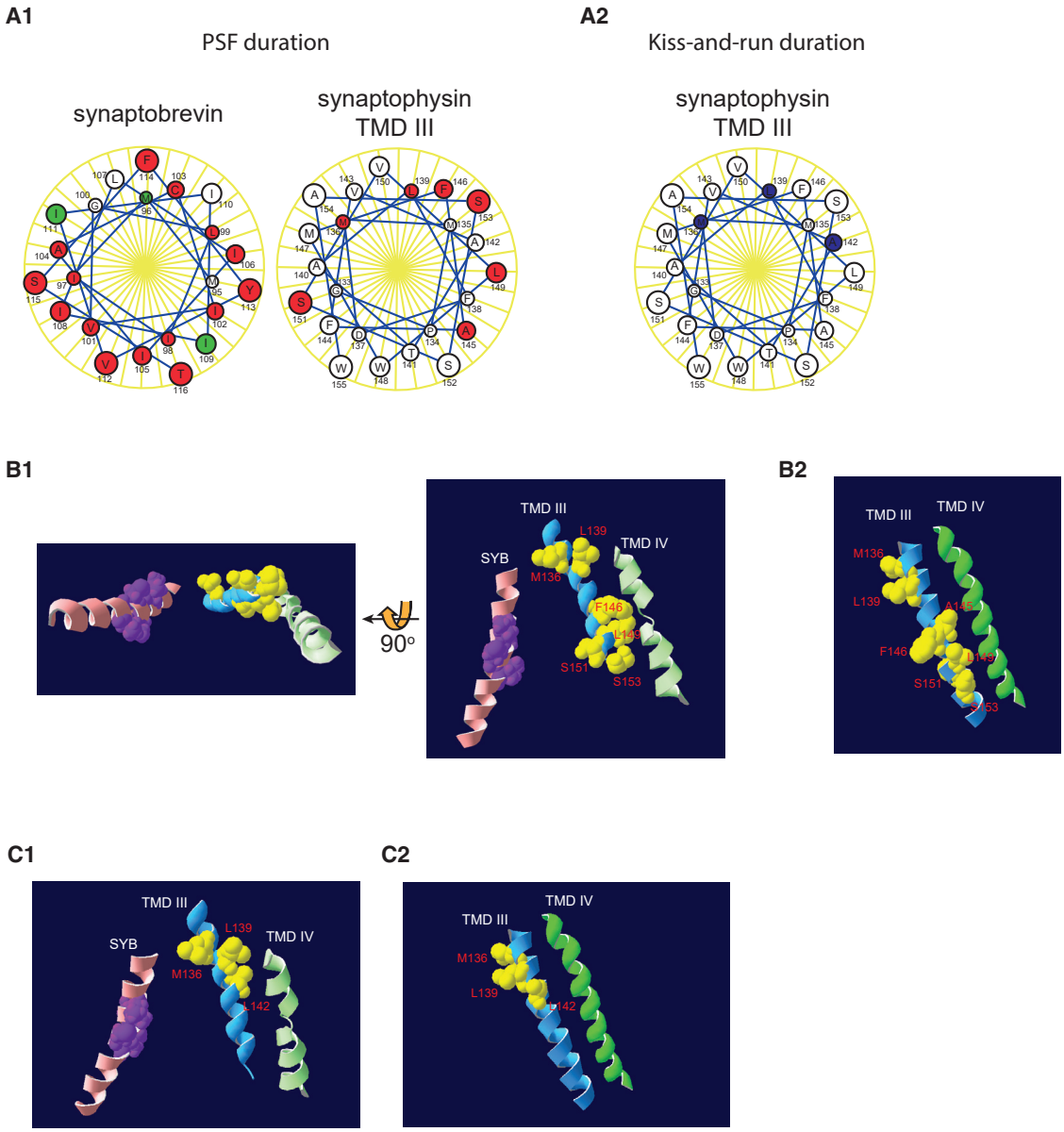

FIGURE 7 TMDs of syp and syb. (*A*1) Helical wheels of syb (*left*) and syp TMD III (*right*). Residues where tryptophan decreased PSF duration are marked in red, and residues where tryptophan increased PSF duration are marked in green. Residues that had no impact or were not tested are white (data for syp are from Fig. 4 and data for syb are from (5)). (*A*2) Helical wheel of syp TMD III highlighting residues that alter kiss-and-run event lifetime (*blue*) from Fig. 3 *C*. (*B*) Structural models of TMDs of syb and syp using a PDB file based on an electron microscopy structure (32) (*B*1) and the AlphaFold database (52) (*B*2) (https://alphafold.ebi.ac.uk/entry/P07825). TMD III (*blue ribbon*), TMD IV (*green ribbon*), and syb (*pink ribbon*) are viewed from outside (*B*1, *left*) and from within the plane of the membrane (*B*1, *right*). Residues of syp TMD III that influence the open time of the fusion pore are highlighted as yellow fills. Putative syb pore-lining residues are purple fills (5). (*C*) TMD III residues (*yellow fills*) that influence the fraction of kiss-and-run events are illustrated in structure models from (32) (*C*1) and from AlphaFold (*C*2) (52).

microscopy structure (32) does not account for our results on fusion pore flux, we also examined a model based on AlphaFold (52) (Fig. 7 *A*2). This model shows more residues facing away from TMD IV (M136, L139, and F146), and they could interact with another molecule such as syb. S153 probably also faces toward syb because in the helical wheel, L139, F146, and S153 are located on the same face (Fig. 7 *A*1). These residues that appear to face toward syb were found to reduce PSF duration (Fig. 4). It should be noted that the syb residues that are potential partners with syp residues are not among those lining the pore (5) (*purple space fills* in Fig. 7 *B*1). These observations suggest that syp TMD III influences initial fusion pore stability by intermolecular interactions with syb as well as intramolecular interactions with other syp TMDs. Future studies of other syp TMDs may provide more insight into how syp regulates fusion pores, and reveal additional functional interactions, with syb and with other proteins of the exocytotic apparatus.

Structural models also aided in the interpretation of changes in release mode. M136, L139, and A142 tryptophan mutants increased the proportion and duration of kiss-and-run events (Fig. 3). Thus, this part of TMD III engages in interactions that impact the stability of early kiss-and-run fusion pores. Fig. 7 *C*1 highlights these three residues in the electron microscopy structure (32). M136 is close to syb, while L139 and A142 are close to syp TMD IV. However, in the AlphaFold model (52), M136 and L139 face away from TMD IV and could potentially face toward syb (Fig. 7 *C*2). Though the orientation of TMD III is different in the two models, both are consistent with the general idea that fusion pores formed during kiss and run are influenced by intermolecular interactions with syb and intramolecular interactions with other syp TMDs.

CONCLUSIONS

TMD III of syp influences the dynamics of initial fusion pores without directly contacting the aqueous pathway taken by catecholamine at the onset of exocytosis. Although these results indicate that the syp-syb complex revealed by electron microscopy (32) is not likely to represent the initial fusion pore, our results suggest an intimate relationship between TMD III and the initial fusion pore that enables this domain to regulate fusion pore activity. Interactions between syp and syb are likely to be important, but the syp TMDs would then surround the pore-lining syb TMDs rather than alternate with them within the pore. The helical face of syb with putative pore-lining residues (highlighted as *purple fills* in Fig. 7 *B*1 and *C*1) is exposed to the pore lumen and inaccessible to contact with a syp TMD. Syp TMDs would then be more likely to interact with a face of syb that is oriented away from the pore lumen.

Our analysis suggests that syp TMD III can regulate fusion pores both by intermolecular interactions with syb and intramolecular interactions with other syp TMDs. A recent study showed that primed synaptic vesicles have a hexameric arrangement of protein density at the interface with the plasma membrane, surrounding the area where the initial fusion pore forms (53). Determining whether syp and syb contribute to this density, where they reside, and how they interact will require more experiments to evaluate the functions of syp and syb in membrane fusion.

AUTHOR CONTRIBUTIONS

Y.-T.H. performed the experiments and analyzed the data. M.B.J. conceived the project. Both authors contributed to the writing.

ACKNOWLEDGMENTS

We thank Che-Wei Chang for discussions and advice. This work was funded by NIH grants R01NS044057 and R35NS127219.

DECLARATION OF INTERESTS

The authors declare no competing interests.

REFERENCES

1. Chow, R. H., L. von Rüden, and E. Neher. 1992. Delay in vesicle fusion revealed by electrochemical monitoring of single secretory events in adrenal chromaffin cells. *Nature.* 356:60–63.
2. Jankowski, J. A., T. J. Schroeder, …, R. M. Wightman. 1993. Temporal characteristics of quantal secretion of catecholamines from adrenal medullary cells. *J. Biol. Chem.* 268:14694–14700.
3. Chiang, C. W., C. W. Chang, and M. B. Jackson. 2018. The transmembrane domain of synaptobrevin influences neurotransmitter flux through synaptic fusion pores. *J. Neurosci.* 38:7179–7191.
4. Bao, H., M. Goldschen-Ohm, …, E. R. Chapman. 2016. Exocytotic fusion pores are composed of both lipids and proteins. *Nat. Struct. Mol. Biol.* 23:67–73.
5. Chang, C. W., E. Hui, …, M. B. Jackson. 2015. A structural role for the synaptobrevin 2 transmembrane domain in dense-core vesicle fusion pores. *J. Neurosci.* 35:5772–5780.
6. Han, X., and M. B. Jackson. 2005. Electrostatic interactions between the syntaxin membrane anchor and neurotransmitter passing through the fusion pore. *Biophys. J.* 88:L20–L22.
7. Han, X., C. T. Wang, …, M. B. Jackson. 2004. Transmembrane segments of syntaxin line the fusion pore of Ca^{2+}-triggered exocytosis. *Science.* 304:289–292.
8. Borisovska, M., Y. Zhao, …, D. Bruns. 2005. v-SNAREs control exocytosis of vesicles from priming to fusion. *EMBO J.* 24:2114–2126.
9. Han, X., and M. B. Jackson. 2006. Structural transitions in the synaptic SNARE complex during Ca^{2+}-triggered exocytosis. *J. Cell Biol.* 172:281–293.
10. Fang, Q., K. Berberian, …, M. Lindau. 2008. The role of the C terminus of the SNARE protein SNAP-25 in fusion pore opening and a model for fusion pore mechanics. *Proc. Natl. Acad. Sci. USA.* 105:15388–15392.
11. Ngatchou, A. N., K. Kisler, …, M. Lindau. 2010. Role of the synaptobrevin C terminus in fusion pore formation. *Proc. Natl. Acad. Sci. USA.* 107:18463–18468.
12. Weiss, A. N. 2019. Synaptobrevin-2 C-Terminal flexible region regulates the discharge of catecholamine molecules. *Biophys. J.* 116:921–929.
13. Bai, J., C. T. Wang, …, E. R. Chapman. 2004. Fusion pore dynamics are regulated by synaptotagmin*t-SNARE interactions. *Neuron.* 41:929–942.
14. Wang, C.-T., R. Grishanin, …, M. B. Jackson. 2001. Synaptotagmin modulation of fusion pore kinetics in regulated exocytosis of dense-core vesicles. *Science.* 294:1111–1115.
15. Wang, C. T., J. C. Lu, …, M. B. Jackson. 2003. Different domains of synaptotagmin control the choice between kiss-and-run and full fusion. *Nature.* 424:943–947.
16. Zhang, Z., E. Hui, …, M. B. Jackson. 2010. Regulation of exocytosis and fusion pores by synaptotagmin-effector interactions. *Mol. Biol. Cell.* 21:2821–2831.
17. Chiang, N., Y. T. Hsiao, …, C. T. Wang. 2014. Phosphomimetic mutation of cysteine string protein-alpha increases the rate of regulated exocytosis by modulating fusion pore dynamics in PC12 cells. *PLoS One.* 9:e99180.
18. Südhof, T. C., F. Lottspeich, …, R. Jahn. 1987. A synaptic vesicle protein with a novel cytoplasmic domain and four transmembrane regions. *Science.* 238:1142–1144.
19. Takamori, S., M. Holt, …, R. Jahn. 2006. Molecular anatomy of a trafficking organelle. *Cell.* 127:831–846.

20. Wilhelm, B. G., S. Mandad, …, S. O. Rizzoli. 2014. Composition of isolated synaptic boutons reveals the amounts of vesicle trafficking proteins. *Science.* 344:1023–1028.
21. González-Jamett, A. M., X. Báez-Matus, …, A. M. Cárdenas. 2010. The association of dynamin with synaptophysin regulates quantal size and duration of exocytotic events in chromaffin cells. *J. Neurosci.* 30:10683–10691.
22. Winkler, H. 1997. Membrane composition of adrenergic large and small dense cored vesicles and of synaptic vesicles: consequences for their biogenesis. *Neurochem. Res.* 22:921–932.
23. Chang, C. W., Y. T. Hsiao, and M. B. Jackson. 2021. Synaptophysin regulates fusion pores and exocytosis mode in chromaffin cells. *J. Neurosci.* 41:3563–3578.
24. McMahon, H. T., V. Y. Bolshakov, …, T. C. Südhof. 1996. Synaptophysin, a major synaptic vesicle protein, is not essential for neurotransmitter release. *Proc. Natl. Acad. Sci. USA.* 93:4760–4764.
25. Eshkind, L. G., and R. E. Leube. 1995. Mice lacking synaptophysin reproduce and form typical synaptic vesicles. *Cell Tissue Res.* 282:423–433.
26. Janz, R., T. C. Südhof, …, V. Y. Bolshakov. 1999. Essential roles in synaptic plasticity for synaptogyrin I and synaptophysin I. *Neuron.* 24:687–700.
27. Kwon, S. E., and E. R. Chapman. 2011. Synaptophysin regulates the kinetics of synaptic vesicle endocytosis in central neurons. *Neuron.* 70:847–854.
28. Arthur, C. P., and M. H. B. Stowell. 2007. Structure of synaptophysin: a hexameric MARVEL-domain channel protein. *Structure.* 15:707–714.
29. Thomas, L., K. Hartung, …, H. Betz. 1988. Identification of synaptophysin as a hexameric channel protein of the synaptic vesicle membrane. *Science.* 242:1050–1053.
30. Betz, H. 1990. Ligand-gated ion channels in the brain: the amino acid receptor superfamily. *Neuron.* 5:383–392.
31. Leube, R. E. 1995. The topogenic fate of the polytopic transmembrane proteins, synaptophysin and connexin, is determined by their membrane-spanning domains. *J. Cell Sci.* 108:883–894.
32. Adams, D. J., C. P. Arthur, and M. H. B. Stowell. 2015. Architecture of the synaptophysin/synaptobrevin complex: structural evidence for an entropic clustering function at the synapse. *Sci. Rep.* 5:13659.
33. Chang, C. W., C. W. Chiang, and M. B. Jackson. 2017. Fusion pores and their control of neurotransmitter and hormone release. *J. Gen. Physiol.* 149:301–322.
34. Cormack, B. 2008. Directed mutagenesis using the polymerase chain reaction. *Curr Protoc Mol Biol Chapter.* 8:Unit8.5.
35. Chow, R. H., and L. von Rüden. 1995. Electrochemical detection of secretion from single cells. *In* Single-Channel Recording. B. Sakmann and E. Neher, eds Plenum Press, New York, pp. 245–275.
36. Jackson, M. B., Y. T. Hsiao, and C. W. Chang. 2020. Fusion pore expansion and contraction during catecholamine release from endocrine cells. *Biophys. J.* 119:219–231.
37. Colliver, T. L., E. J. Hess, …, A. G. Ewing. 2000. Quantitative and statistical analysis of the shape of amperometric spikes recorded from two populations of cells. *J. Neurochem.* 74:1086–1097.
38. Ren, L., L. J. Mellander, …, A. G. Ewing. 2016. The evidence for open and closed exocytosis as the primary release mechanism. *Q. Rev. Biophys.* 49:e12.
39. Hu, R., B. Ren, …, C. Amatore. 2016. How "full" is "full fusion" during exocytosis from dense core vesicles? Effect of SDS on "quantal" release and final fusion pore size. *J. Electrochem. Soc.* 163:H853–H865.
40. Alvarez de Toledo, G., R. Fernández-Chacón, and J. M. Fernández. 1993. Release of secretory products during transient vesicle fusion. *Nature.* 363:554–558.
41. Zhou, Z., S. Misler, and R. H. Chow. 1996. Rapid fluctuations in transmitter release from single vesicles in bovine adrenal chromaffin cells. *Biophys. J.* 70:1543–1552.
42. Chang, C. W., Y. T. Hsiao, …, M. B. Jackson. 2022. Full-fusion and kiss-and-run in chromaffin cells controlled by irreversible vesicle size-dependent fusion pore transitions. *Cell Calcium.* 105:102606.
43. Edelmann, L., P. I. Hanson, …, R. Jahn. 1995. Synaptobrevin binding to synaptophysin: a potential mechanism for controlling the exocytotic fusion machine. *EMBO J.* 14:224–231.
44. Sugita, S., R. Janz, and T. C. Südhof. 1999. Synaptogyrins regulate Ca2+-dependent exocytosis in PC12 cells. *J. Biol. Chem.* 274:18893–18901.
45. Raja, M. K., J. Preobraschenski, …, J. F. Wesseling. 2019. Elevated synaptic vesicle release probability in synaptophysin/gyrin family quadruple knockouts. *Elife.* 8:e40744.
46. Stevens, R. J., Y. Akbergenova, …, J. T. Littleton. 2012. Abnormal synaptic vesicle biogenesis in Drosophila synaptogyrin mutants. *J. Neurosci.* 32:18054–18067.
47. Abraham, C., H. Hutter, …, R. E. Leube. 2006. Synaptic tetraspan vesicle membrane proteins are conserved but not needed for synaptogenesis and neuronal function in Caenorhabditis elegans. *Proc. Natl. Acad. Sci. USA.* 103:8227–8232.
48. Gordon, S. L., and M. A. Cousin. 2014. The Sybtraps: control of synaptobrevin traffic by synaptophysin, alpha-synuclein and AP-180. *Traffic.* 15:245–254.
49. Chang, C. W., and M. B. Jackson. 2015. Synaptobrevin transmembrane domain influences exocytosis by perturbing vesicle membrane curvature. *Biophys. J.* 109:76–84.
50. Calakos, N., and R. H. Scheller. 1994. Vesicle-associated membrane protein and synaptophysin are associated on the synaptic vesicle. *J. Biol. Chem.* 269:24534–24537.
51. Becher, A., A. Drenckhahn, …, G. Ahnert-Hilger. 1999. The synaptophysin-synaptobrevin complex: a hallmark of synaptic vesicle maturation. *J. Neurosci.* 19:1922–1931.
52. Jumper, J., R. Evans, …, D. Hassabis. 2021. Highly accurate protein structure prediction with AlphaFold. *Nature.* 596:583–589.
53. Radhakrishnan, A., X. Li, …, J. E. Rothman. 2021. Symmetrical arrangement of proteins under release-ready vesicles in presynaptic terminals. *Proc. Natl. Acad. Sci. USA.* 118:e2024029118.